Laser-induced ignition and subsequent flame development along five co-planar monodisperse fuel droplet streams

T. Mosbach*, G.C. Gebel and W. Meier
Institute of Combustion Technology, German Aerospace Center (DLR), Stuttgart, Germany
thomas.mosbach@dlr.de and gregor.gebel@dlr.de

Abstract

This study reports about experiments performed at a generic lab-scale combustor under well-defined boundary conditions contributing to the today's knowledge base of the spray ignition process. The combustor consists of a flow channel and a vibrating orifice monodisperse droplet injector generating five co-planar monodisperse fuel droplet streams. The fuel sprays were ignited with focused laser radiation to provide well-defined ignition conditions. The development of the laser-induced plasma, the subsequent flame kernel formation and the growth and propagation of the initial flame were investigated for different fuels and combustor operating conditions. High-speed imaging, planar laser induced fluorescence, particle image velocimetry and optical spectroscopy techniques were applied to provide a comprehensive data set for the development and validation of numerical models of the flame initiation process.

Introduction

The ignition of fuel sprays is of great fundamental and practical interest in combustion. Spray combustion is employed in various practical systems and ignition is often a crucial operational requirement of these systems. A successful ignition of a spray flame involves the formation of a self-sustainable flame kernel, followed by the propagation and growth of an initial flame and finally followed by the establishment of a stably burning flame in the flow [1, 2]. Therefore, the transient flame initiation process is subjected to various mechanisms.

While the ignition process of gaseous fuel/air mixtures is widely studied [2-4], studies on spray ignitions are still scarce [5-6]. However, a deep understanding of the relevant processes is essential for the development and validation of numerical models of the flame initiation in multi-phase flows. Especially, a good understanding of the phenomena, which occur during the flame kernel formation phase, is a key requirement to adequately select numerical models and boundary conditions for simulations starting after the establishment of a flame kernel. Moreover, in order to verify the results of simulations adequate validation data for the initial flame phase are also required. These data are especially important to validate the evaporation predictions of numerical models for multicomponent fuels.

Simplified generic experiments are needed not only to provide well-defined boundary conditions and adequate validation data for numerical simulations but also to gain increased understanding of the relevant spray ignition processes. This study reports about experiments performed at a generic lab-scale combustor. The combustion chamber consists of a flow channel with simplified geometry; the measurements were performed at atmospheric pressure. A well-defined two-dimensional spray consisting of five co-planar streams of monodisperse fuel droplets was generated by an appropriate injector in the flow channel. The droplet-laden flow was ignited with focused laser radiation in order to provide also well-defined ignition conditions. In particular, the ignition energy, location, and start time can be accurately adjusted using a laser ignition system. As mentioned before studies on spray ignitions are scarce, however to the best of our knowledge no studies of the laser-induced flame initiation process in two-phase fuel/air flows are available in the literature.

Optical and laser-based measurement techniques are suited to capture the transient flame initiation process with high temporal and spatial resolution. In this study high-speed imaging of the broadband luminosity was used to capture the growth and propagation of the initial flame following the laser-induced flame kernel. The kerosene fuel and hydroxyl radical (OH) density distribution were simultaneously measured using the planar laser-induced fluorescence (PLIF) technique. In general, with this technique the influence of the fuel placement and the influence of the position and shape of the reaction zones and regions of high temperature on the flame initiation process can be studied. Particle image velocimetry (PIV) measurements were performed to characterize the air co-flow as it is an important parameter for the flame development. The phenomena related to the flame kernel formation process were investigated by high-speed imaging and optical emission spectroscopy techniques.

The measured set of experimental data was employed to validate numerical simulations of our combustor configuration at the DLR [7, 8].

* Corresponding author: thomas.mosbach@dlr.de

Experimental Methods

Combustor and ignition laser

The experiments were performed at a generic lab-scale combustor under well-defined boundary conditions. The main components of the combustor are a flow channel and a vibrating orifice monodisperse fuel-droplet generator. The flow channel has a nearly squared cross-section with an area of 62 cm^2 along its length of one meter. Good optical accessibility of the ignition and combustion region is given for optical measurement techniques. The fuel-droplets are injected by a modified piezoelectric driven vibrating orifice aerosol generator (TSI VOAG 3450). The droplet generator head was equipped with a laser perforated orifice with five co-planar micro-holes (diameter 50 µm, center-to-center distance 1050 µm) and was placed in the upper-half of the flow channel, injecting monodisperse fuel-droplet streams in direction of the air co-flow. The two-dimensional droplet loads in the combustor were ignited by focused laser radiation from a frequency-doubled, flash-lamp pumped, solid-state Nd:YAG laser (InnoLas Spitlight 600-10). This laser produced pulse energies of up to 400 mJ at 532 nm.

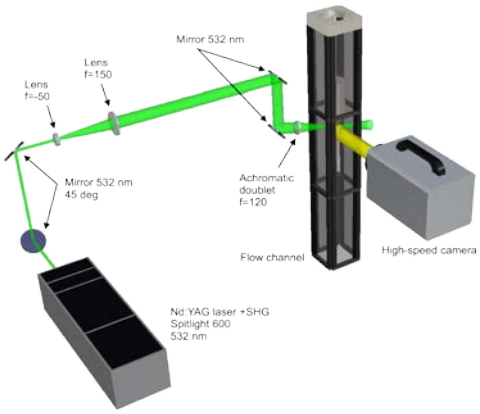

Figure 1 Experimental set-up for high-speed imaging of the broadband luminosity.

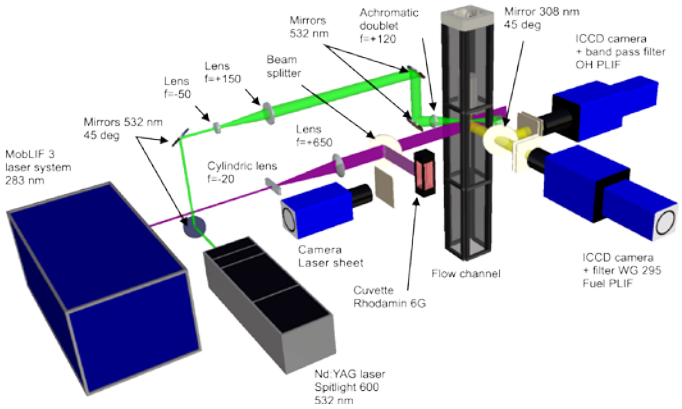

Figure 2 Set-up for the simultaneous PLIF measurements of the kerosene and OH density distribution

Measurements at the generic combustor were conducted at atmospheric pressure for different fuels and test-rig operating conditions, e.g. fuel and air mass flow rates. The following fuels were investigated: Jet A-1 kerosene, a binary mixture of 80 vol.-% n-decane and 20 vol.-% n-propylbenzene (a kerosene surrogate), n-heptane, ethanol, and Exxsol D80. Fuel mass flow rates ranged from 1.8 g/min up to 7 g/min. The fuel was kept at a constant temperature of 21°C. The air co-flow temperature was measured to about 290 K by thermocouples.

Optical and laser-based measurement techniques

Figure 1 displays a schematic of the experimental set-up for high-speed broadband luminosity imaging. A high-speed CMOS camera (LaVision HighSpeedStar 5) equipped with a Nikon lens (type Nikkor MF, f/1.4, f=85 mm) was arranged perpendicularly to the flow direction, providing luminosity images at a repetition rate of 3 kHz of the flame initiation process and of the flame. The camera resolution was set to 1024 x 1024 pixels and the exposure time was set between 1/3000 and 1/40000 seconds depending on the speed and luminescence of the observed phenomena. The field-of-view was determined using a test-target to 66.6 x 66.6 mm.

Figure 2 shows the experimental set-up for the simultaneous planar laser-induced fluorescence (PLIF) measurements of the kerosene and OH distributions. Tuneable, pulsed ultraviolet laser radiation was provided by a frequency-doubled, flash-lamp pumped, solid-state Nd:YAG laser (Spectra-Physics PIV-400-10) pumping a tuneable dye laser (Sirah PRSC-G-24-EG) at 10 Hz repetition rate. The dye laser was tuned to the $Q_1(5)$ transition at approximately 283 nm within the vibrational band v"=0, v'=1 of the OH $A^2\Sigma^+$-$X^2\Pi$ system. A small portion of the laser beam was deflected into a methane-air reference flame stabilized on a matrix burner. The reference flame was used for verifying the excitation line position. An appropriate set of optics were used to expand the laser beam into a vertical sheet as indicated in Figure 2. A beam splitter deflected a small fraction of the laser sheet into a quartz cell filled with fluorescent dye solution (Rhodamine 6G in ethanol). The dye cell fluorescence profile was recorded by a CCD camera (LaVision Imager Intense 3) and was used for correcting non-uniformities of the laser sheet profile. The laser sheet inside the flow channel was 92 mm in height and approximately 0.5 mm in thickness. The OH and the kerosene fluorescence were simultaneously imaged by two camera systems of the same type (LaVision Imager Intense 3 with image intensifier IRO 25). Both camera systems were equipped with Nikon UV-lenses (type Nikkor f/4.5, f =105mm).

The OH fluorescence in the v '=1, v "=1 and v '=0, v "=0 bands near 310 nm was deflected to the cameras by a custom-built high-reflecting mirror in order to reduce the fuel fluorescence contribution (and also near in-

frared radiation) and was finally detected through two interference filters with peak transmission at 310 nm. The fuel fluorescence in the spectral range from 310 to 420 nm (with a maximum around 340 nm) passed through the dichroic mirror reflecting the OH fluorescence and was detected through two Schott WG295 filters. The images were recorded at a sustained repetition rate of 5 Hz. The gates of both image intensifiers were set to 200 ns. The field-of-view of was 68.5 x 90.9 mm.

The experimental set-up for the PIV measurements is displayed in Figure 3. Pulsed laser radiation at 532 nm was provided by a frequency-doubled, flash-lamp pumped, solid-state Nd:YAG laser (model InnoLas Spitlight 600-10). The laser beam was expanded to a vertical sheet with a height of 59 mm and a thickness of about 1 mm. A CCD camera (LaVision Imager Intense 3) equipped with a Nikon lens (AF Nikkor 50 mm 1:1.8D) was arranged perpendicular to the laser sheet plane. The co-flow through the flow-channel was seeded with non-coated titanium-dioxide particles (average diameter 1 µm). For this purpose, a fraction of the air inflow was bypassed through a fluidized bed particle seeder (LaVision) into the flow channel. The laser and the camera were set in a double-pulse mode, respectively double-frame mode at 5 Hz repetition rate. Double-pulse separation times ranged from 180 to 400 µs, depending on the flow conditions. 500 double frames were recorded per measurement with a resolution of 1376 x 1040 pixels per frame. For each flow rate, three measurements at different vertical positions in the flow channel were performed by vertically relocating the flow channel, using its translation stage.

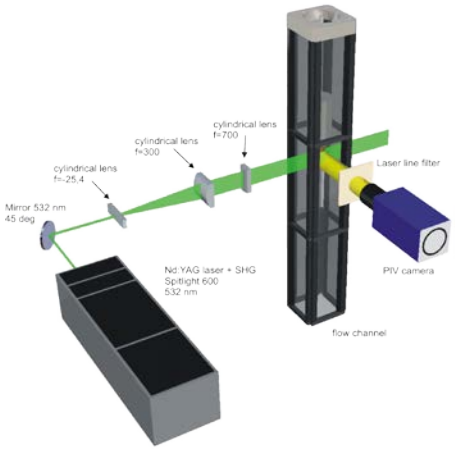

Figure 3 Experimental set-up for the PIV measurements at 5 Hz repetition rate.

The experimental set-ups for the high-speed broadband luminosity imaging and optical emission spectroscopy of the laser-induced ignition process are provided in detail in [6]. Therefore, only a short overview is given here. The set-up for the luminosity imaging was similar to the set-up displayed in Figure 1: A high-speed CMOS camera (LaVision HighSpeedStar 6) was arranged perpendicularly to the flow direction provided broadband luminosity images at a repetition rate of 250 kHz, an exposure time of 1 µs and a resolution of 128 x 80 pixels. Multiple recordings at different starting times were performed in order to gain a higher temporal resolution. For the optical emission spectroscopy an Echelle spectrometer (LLA Instruments ESA 4000 EV/i) with a spectral sensitivity range from 200 to 780 nm was used. Multiple spectra were recorded at various exposure and starting times in order to capture the various light emissions of the phenomena.

Results and Discussion

High-speed broadband luminosity imaging

High-speed broadband luminosity imaging was applied to investigate the overall development of the initial flame and its initiation process. Here, the spectral and line-of-sight integration of the flame luminosity has to be taken into account. The natural flame emission spectrum is comprised primarily of the chemiluminescence spectrum of the different intermediate combustion radicals and of the gray/blackbody continuous thermal radiation from soot and other particulates. In our case, the spectrally integrated natural flame emission from 350 nm to about 1000 nm was imaged. The wavelength range was defined by the optical material of the lens and by the spectral sensitivity of the CMOS image sensor.

The laser used for ignition was operated in a single shot mode and produced pulse energies of 320 mJ at 532 nm. The laser was focussed 10 mm below the injector head on the fuel droplet streams. These ignition conditions were kept constant for all measurements. Moreover, for all combustor operating conditions, the droplet diameter (97 ± 0.8 µm) and the center-to-center distance (244 ± 6 µm) between consecutive droplets were kept constant, as well. Higher fuel flow rates resulted solely in higher droplet velocities (velocities ranged from 4 to 18 m/s) and therefore in a higher axial impulse of the fuel flow. Due to the short time scale (10 µs) of the laser-induced spark, the low air co-flow velocities (less than 1 m/s), and the moderate droplet velocities, the influenced volume of fuel and air was approximately constant for the measurements performed in this study. Therefore, at each ignition, approximately the same number of droplets (that was 240 ± 10), and thus the same fuel volume (0.107 - 0.122 mm³) was disintegrated or evaporated by the laser-induced ignition process. Because of the similar densities of the investigated fuels, the influenced mass of fuel was also approximately constant. However, even for the same ignition and combustor operating conditions differences in the growth and propaga-

tion of the initial flame following the flame kernel formation were observed revealing a stochastic process, as expected especially for multicomponent fuels.

Ethanol showed the least stochastic scatter from ignition to ignition. In addition to the differences in the spatial and temporal development of the flame kernel and the flame between the different fuels, strong differences in the volume-averaged luminous intensity were observed (not shown here). Ethanol showed the least luminous intensity, the intensity of n-heptane was twice of the intensity of ethanol. Kerosene Jet A-1 and the kerosene surrogate showed a luminous intensity which was two orders of magnitude higher than the measured intensity of ethanol.

Figure 4 shows the temporal development of the axial-position (the y-position) of the detected lower flame edge downstream the injector head during the first ten to thirty milliseconds. The droplets were injected at the position y=0. Exemplary results are displayed for ethanol and Jet A-1 kerosene. The bands reflect the different measured positions of the flame edge at constant fuel mass flow but different air mass flows (78 to 776 g/min) at a certain time after ignition. Each band contains the averaged information from 20 up to 40 ignitions. From these graphs the tendency is clearly seen that the corresponding lower flame edge velocity increases with increasing fuel mass flow. Moreover, the figure shows that the flame edge velocities of ethanol are higher than the flame edge velocities of Jet A-1. In order to accurately investigate these effects the measured local flame edge positions were corrected by removing the influence of the air flow-field downstream the injector head. The flow-field characteristic was determined from the PIV measurement results – see below.

Figure 5 shows the dependence of the lower flame edge velocities on the global fuel-to-air ratio (FAR) for different fuels and fuel mass flows. The corrected measured flame edge velocities range from 0.2 to 3.4 m/s and show a clear dependency on the FAR and on the fuel mass flow. The influence of the fuel mass flow on the lower flame edge velocities is considerably lower for ethanol than for the other fuels.

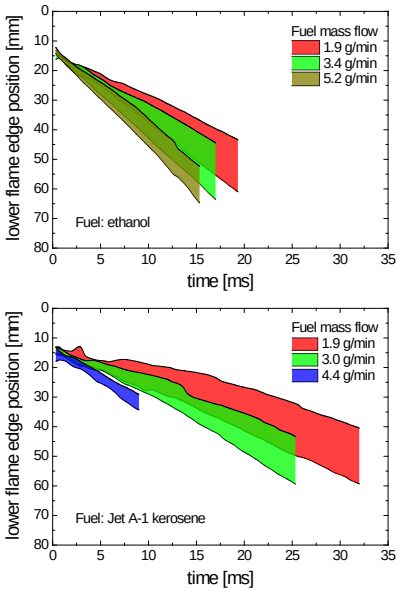

Figure 4 Temporal development of the axial-position of the lower flame edge. Fuels: Ethanol and Jet A-1.

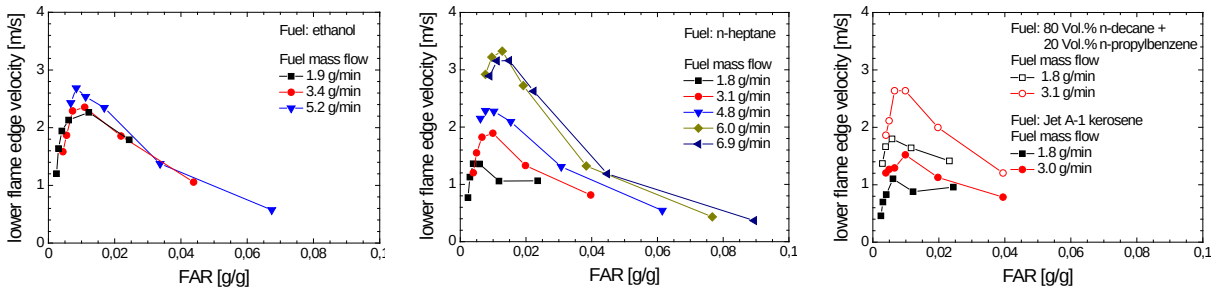

Figure 5 Dependence of the lower flame edge velocities on the global fuel-to-air ratio (FAR) for different fuels and fuel mass flows.

Planar laser-induced fluorescence measurements

In order to obtain information about the local fuel and hydroxyl radical (OH) density distribution, simultaneous kerosene and OH planar laser-induced fluorescence (PLIF) measurements were conducted at the generic lab-scale combustor. The PLIF measurement system was triggered relative to the ignition start. Typical time delays for the temporal scanning of the flame initiation process were 0.5, 1, 1.5, 2, 3, 4, 5, 6, 8, 10, 15, 20, 30 and 40 milliseconds, respectively. For each delay the measurements were repeated several times for the statistical analysis.

The images displayed in Figure 6 are representative instantaneous images from the set of images recorded at the following time delays: 0.5, 2, 6, and 40 milliseconds, top down respectively. Note that some of the displayed images are cut-outs from the full-size images. The fuel was Exxsol D80 kerosene, which has a considerably lower content of aromatics compared to Jet A-1 kerosene. The combustor operating conditions were: Air mass coflow of 465 g/min, fuel mass flow of 1.93 g/min and fuel temperature of 21°C. Each pair of images shows the fuel fluorescence on the left-side and the OH fluorescence on the right-side in the presence of the five droplet streams. The focused ignition laser beam traversed the flow channel from the left side at an angle of approxi-

mately 45 degrees to the flow direction. The density distribution of the OH molecules reflects both the position and shape of the reaction zone and regions of high temperature.

Note that the signal contribution from the droplets in the OH PLIF images is no OH fluorescence but rather fuel fluorescence. It is challenging to eliminate this signal contribution, because of its strength and spectral emission range, which overlaps with the OH spectral emission range. In all images shown here, the fluorescence signal from the droplets (from the liquid phase) was reduced by a numerical post-processing method.

The reaction zones appear in the instantaneous OH PLIF images as band structure. Fuel droplets passing the flame were observed. The fuel vapor produced by the ignition process is clearly seen in the fuel PLIF images. It can be assumed that the initial temperature of the local fuel/air mixture is very high allowing spontaneous ignition to occur. Note that all fuel molecules within the laser-induced plasma core were fully disintegrated. Therefore, we have not only evaporated fuel in the flame kernel area but also smaller combustible molecules and radicals formed in the decaying plasma by atomic recombination processes. These additional plasma-generated molecules can possibly support initial flame reactions.

Comparison of the OH and fuel PLIF images evidence that the reaction zones surround the measured area of fuel vapor. Obviously, the fuel vapor area must be very rich, preventing flame reactions in which OH is formed. Outside, the fuel/air mixture is too lean and cold, preventing flame reactions, as well.

In summary the PLIF measurements of the fuel and OH density distributions show an initial diffusion flame growing and propagating along the fuel droplet streams. The unburned gaseous fuel is surrounded by a three-dimensional closed thin flame-front and the oxidizer comes from outside. In the beginning, the flame combusts mainly the fuel vapor generated by the ignition process. After about 10 ms, the flame evaporates and combusts the liquid fuel. At times greater than about 40 ms the emission signatures as seen in the instantaneous kerosene PLIF images have changed: The fuel vapor distribution seems to be influenced by thermal convection.

The position of the ignition influenced area in the droplet streams is very reproducible; it is conserved in the flow and can be tracked. The left graph of Figure 7 shows the lower edge position of the ignition influenced area as function of time for three different operating conditions. From the slope of the curves the initial droplet velocity at the injector head was derived. These velocities are in a good agreement with the velocities as determined from the theoretical consideration of Rayleigh breakup of fuel jets.

Image averaging was performed over each set of instantaneous images for a given time delay in order to quantify the flame growth and propagation. In the averaged images (not shown here) the overall temporal

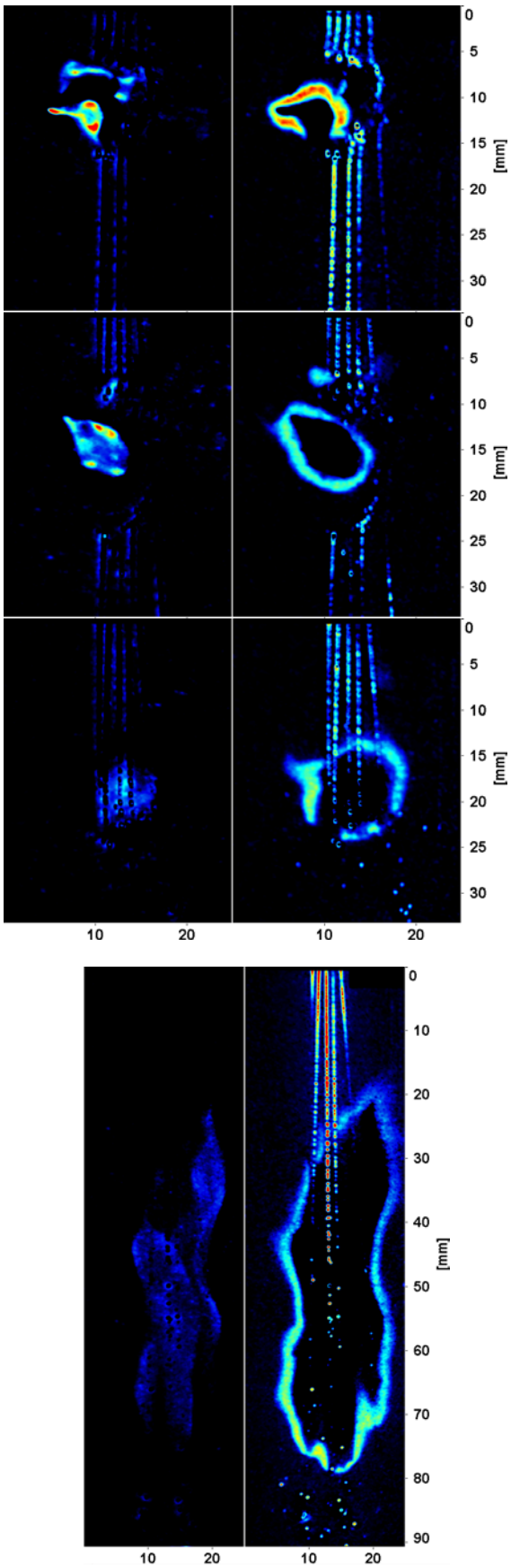

Figure 6 Instantaneous images of the fuel (on the left) and OH (on the right) density distribution recorded at the time delays: 0.5, 2, 6, and 40 ms (top down).

development of the averaged fuel vapor and OH distributions are more clearly seen. The extension of the density distributions stays in the order of ten millimeters within the first ten milliseconds after ignition for the different investigated combustor operating conditions. From the averaged OH PLIF images the centroid of the OH density distribution was determined. The results are plotted in the right graph of Figure 7 for three operating conditions. The corresponding volume averaged velocities in downstream direction derived from the slope of the curves are depending on both the fuel mass flow and on the air co-flow. The velocities have a typical magnitude of 1 m/s, which is in excellent agreement with the results of the numerical simulation of this experiment [7].

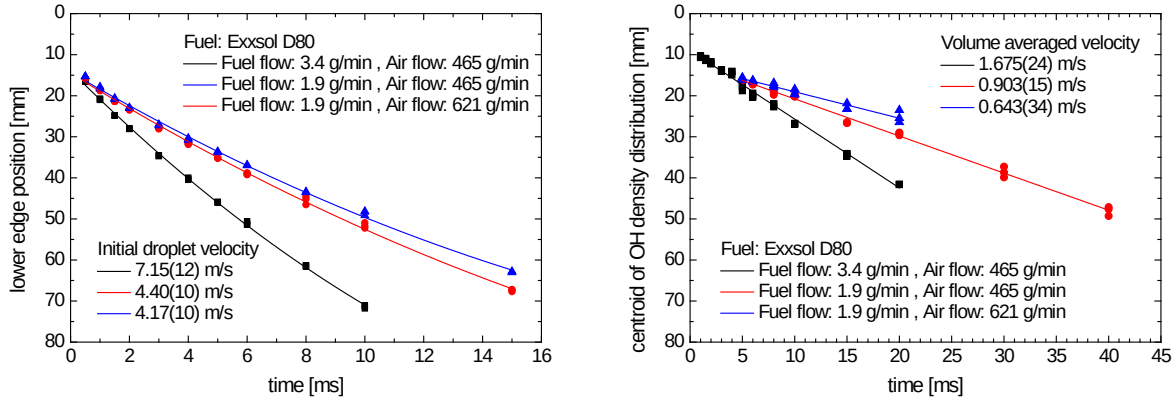

Figure 7 Temporal development of the axial-position of the lower edge of the ignition-influenced area (left Graph) and the centroid of the OH density distribution (right Graph) for three different operating conditions.

Ignition probability

An ignition probability study was carried out to find the dependencies on the fuel and air mass flow and on the laser pulse energy. The ignition probability increases, as expected, for laser energies above the threshold energy until a constant ignition probability is reached. The determined ignition probability decreases strongly with the fuel mass flow and depends only slightly on the co-flow for air flows above a certain minimum value. Ignition was only possible by focusing the laser radiation into the droplet stream. A focus outside the region of the droplet streams resulted in an almost zero ignition probability. This suggests that the amount of evaporated fuel is below the ignition limit. Numerical simulations of this experiment [7-8] confirmed that without the quasi-instantaneous phase change there would initially not be enough evaporated fuel to sustain the flame kernel under the given time scales and boundary conditions.

Investigation of the laser-induced breakdown

In order to investigate the phenomena related to the ignition process through a laser-induced breakdown the following measurement techniques were applied at high repetition rates at our specific experimental configuration: broadband luminosity imaging, optical emission spectroscopy and Schlieren imaging. Since these results were already published [9], only the main findings are summarized in the following: The breakdown plasma grows rapidly during the first 1.5 µs; afterwards it expands in direction of the incident laser beam. The breakdown is the origin of a spherically expanding blast wave. The blast wave trajectories in static air and in a droplet-laden flow are identical, when the breakdown energy and the air pressure are the same. Initially, the breakdown plasma is optically thick as indicated by the decaying broadband thermal emission spectrum in the first 0.5 µs. Transition to optically thin plasma occurs after about 50 ns as ionic nitrogen and oxygen lines become detectable in the emission spectrum. Nitrogen, oxygen and carbon atoms and excited CN* and C_2* molecules from recombination processes are observed after several hundred nanoseconds. CN* and C_2* reveal dissociation of the hydrocarbon molecules. CH* from initial combustion reactions is observed not earlier than 0.1 ms after ignition start. OH* was not detected due to the limited sensitivity of the optical setup in the ultraviolet spectral range.

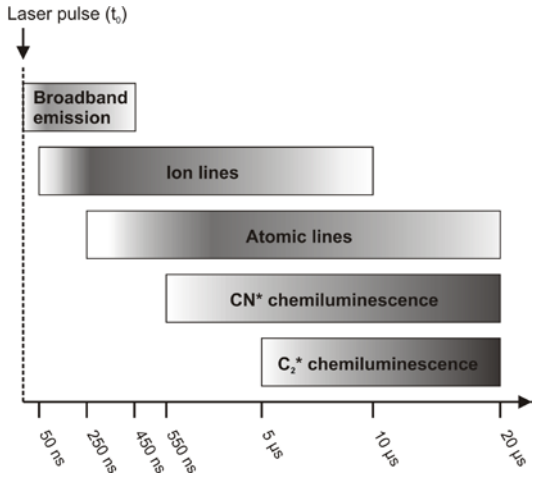

Figure 8 Phases of the decaying laser-induced plasma respectively of the flame kernel.

The ignition process is stated according to the foregoing information as follows: At the given operating conditions, in particular the initial droplet size and the fuel and air temperature, the fuel vapor in the region of the laser-ignition is far below the flame ignition limit. Fuel vapor and radicals necessary for the flame initiation are produced during the ignition process. A flame kernel is established in the droplet-free region generated by the laser ignition process. The subsequent initial diffusion flame propagates downstream along the fuel-droplet streams with a velocity lower than the droplet velocity and is consuming the fuel vapor generated by the ignition process. Fuel droplets can enter and traverse the initial flame. Along the droplet streams, free radicals are removed from the flame, the oxidizer is displaced and the flame front is locally disturbed by the droplet-induced shear flow layers. Due to the short residence time of the fuel droplets in the flame, the droplets are even able to pass the flame, thus removing heat from the initial flame. Therefore, a successful ignition in our specific experimental configuration depends not only on the initial heat dissipation, e.g. the thermal area loading, and vapor and radical formation but possibly also on the droplet velocity, e.g. the droplet residence time in the flame and the strength of the induced shear flow layers around the droplet streams.

Particle image velocimetry

Laser-based flow field measurements using the particle image velocimetry technique (PIV) were performed at the generic lab-scale combustor without fuel injection, for air mass flows between 259 and 1034 g/min. The objective was to characterize the air co-flow around and below the droplet generator. Post-processing of the recorded images was performed with the FlowMaster module of the software DaVis 7.2 from LaVision. Figure 9 shows a streamline map of an averaged flow field for an air mass flow of 776 g/min. The local in-plane velocities are color-mapped (Red: high velocities, Blue: low velocities).

A recirculation zone downstream of the injector head, with a toroidal vortex rotating at low velocities, is clearly seen. Two further toroidal vortices are located around the injector head and in the gap between head and liquid chamber base of the TSI droplet generator. As a result of the injector narrowing the flow channel cross-section, high flow velocities are observed in the fringe area of the flow field downstream of the injector. Velocity gradients in radial direction decrease with increasing distance to the injector, but considerable velocity gradients still exist. However, the radial velocity component and the gradient of the radial velocity are at a minimum in the core area, where the ignition and initial flame propagation take place. This area of low flow velocities downstream of the injector head is of particular interest. The graphs of Figure 10 show cross-stream and down-stream averaged axial velocities for different air mass flows. Averaging was performed from -10 to +10 mm in cross-stream direction and down-stream from the injector head to the end of the observed flow field. The graph on the left displays the cross-stream averaged axial velocities within the recirculation zone. The minimum represents the center of the toroidal vortex; its size and therefore the size of the recirculation zone increases with increasing air co-flow. The graph on the right shows parabolic flow profiles in the down-stream average with low air-flow velocities close to the injector axis. The observed asymmetries at the lower flow mass rates are clearly decreasing with increasing flow rate.

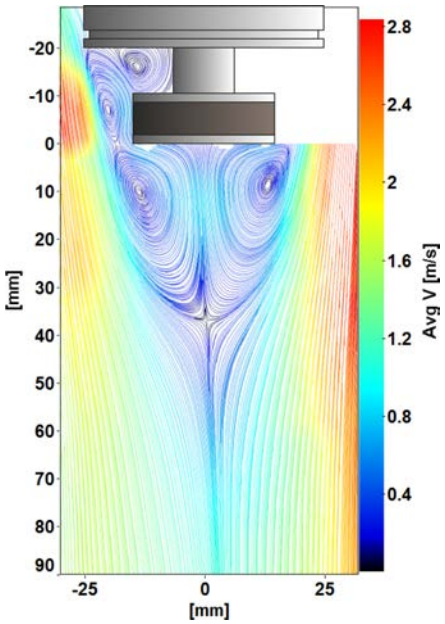

Figure 9 Exemplary streamline map of an averaged flow field.

High-speed PIV at 5 kHz repetition rate was also applied to monitor flow unsteadinesses with high temporal resolution, but is not presented here.

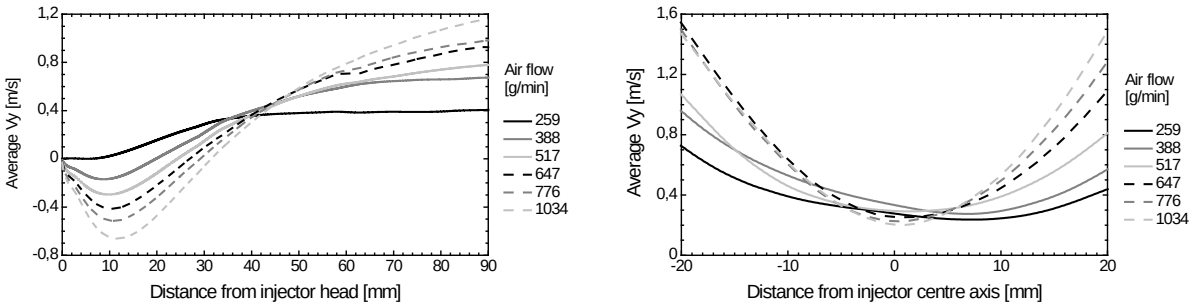

Figure 10 Dependence of the cross-stream and down-stream averaged axial velocities on the air mass flow.

Summary and Conclusions

The flame initiation in a two-dimensional monodisperse spray was investigated by applying optical and laser-based measurement techniques. Detailed description of the diagnostic methods was provided. The experiments were performed at a generic lab-scale combustor under well-defined boundary conditions. The combustor consists of a flow channel and a monodisperse droplet injector generating five co-planar monodisperse streams of fuel droplets. The droplet diameter was about 100 micrometers.

The fuel/air two-phase flow was ignited by focused laser radiation to provide well-defined ignition conditions. It was pointed out that the area influenced by the ignition process was identical for all measurements performed during this study. Approximately the same number of droplets were evaporated or disintegrated during the laser-induced ignition process.

Broadband luminosity imaging measurements were performed to track the axial-position of the lower edge of the initial flame during the first ten to thirty milliseconds. Differences in the growth and propagation of the initial flame following the flame kernel formation were observed for identical ignition and combustor operating conditions revealing a stochastic process. It was found that the average lower edge velocity of the initial flame increases with increasing fuel mass flow.

The PLIF measurements of the fuel and OH density distributions evidence a diffusion flame propagating along the monodisperse fuel-droplet streams. The unburned gaseous fuel is surrounded by a three-dimensional closed thin flame-front and the oxidizer comes from outside. The flame propagates downstream with a velocity lower than the droplet velocity. Fuel droplets can enter and traverse the flame fronts of the initial flame. Therefore, a successful ignition in our specific experimental configuration depends not only on the initial heat dissipation, e.g. the thermal area loading, radical and fuel vapor formation but possibly also on the droplet velocity, e.g. the droplet residence time in the flame and the strength of the induced shear flow layers around the droplet streams.

The position of the area influenced by the ignition process in the droplet streams is very reproducible; it is conserved in the flow and can be tracked. The initial droplet velocity at the injector head was derived from the slope of the trajectory of the lower edge position of the influenced area. From the averaged OH PLIF images the centroid of the OH density distribution was determined. The corresponding centroid velocities in downstream direction depend on both the fuel flow and on the air co-flow. The velocities have a typical magnitude of 1 m/s.

The PIV measurement results provide quantitative information about the actual flow-field at the different combustor operating conditions without fuel injection. The flow-field in the region, where the ignition and initial flame propagation take place is of particular interest. The radial velocity component and the gradient of the radial velocity of the air-flow are at a minimum in this region. Therefore, the fuel droplet streams are not displaced from their initial trajectory.

This study revealed several findings about the complex processes during the flame initiation. The results provide a valuable data set for the development and validation of numerical models of spray ignition.

Acknowledgements

This work received funding from the European Community through the project TIMECOP-AE (Project# AST5-CT-2006-030828). It reflects only the author's views and the Community is not liable for any use that may be made of the information contained therein.

References

[1] Lefebvre, A.H., Ballal, D.R., *Gas Turbine Combustion*, Taylor & Francis, 3rd Edition, 2010.
[2] Mastorakos, E., *Progress of turbulent non-premixed flames* 35: 57-97 (2009).
[3] Bradley, D., Sheppard, C.G.W., Suardjaja, I.M., and Woolley, R., *Combustion and Flame* 138: 55-77 (2004).
[4] Phuoc, T.X., *Optics and Lasers in Engineering* 44: 351-397 (2006).
[5] Aggarwal, S.K., *Progress in Energy and Combustion Science* 24: 565-600 (1998).
[6] Marchione, T., Ahmed, S.F., and Mastorakos, E., *Combustion and Flame* 156: 166-180 (2009).
[7] Boyde, J., Le Clercq, P., Di Domenico, M., Mosbach, T., Gebel, G.C., Rachner, M., and Aigner, M., *Proceedings of the 49th AIAA Aerospace Science Meeting*, Orlando, Florida, January 4 - 7, 2011.
[8] Boyde, J., Le Clercq, P., Di Domenico, M., Rachner, M., Gebel G.C., Mosbach, T., and Aigner, M., *Proceedings of the ASME Turbo Expo 2011*, Vancouver, Canada, June 6 - 10, 2011.
[9] Gebel, G.C., Mosbach, T., Meier, W., and Aigner, M., *Proceedings of the 50th European Combustion Meeting*, Cardiff, June 28 - July 01, 2011.